Raman and Brillouin spectroscopic studies of CH_4 single crystals in phases I and II

E. Gregoryanz, M. J. Clouter, N. H. Rich, and R. Goulding
Department of Physics and Physical Oceanography, Memorial University of Newfoundland, St. John's, Newfoundland, Canada A1B 3X7
(Received 21 January 1998)

A technique has been developed for obtaining single crystals of solid methane in phase II which can be reached only from within phase I at zero pressure. Large ($\sim$50 mm^3) single crystals of CH_4-I were grown in a cylindrical quartz cell and successfully cooled below the phase-transition temperature. Brillouin spectra were collected at different crystal orientations corresponding to rotation about the laboratory z axis. X-ray Lauë diffraction techniques were applied to determine the orientation of the crystals in the laboratory frame. The elastic constants of CH_4-I were determined as a function of temperature from 90 to 20.5 K and the elastic constants of CH_4-II were determined as a function of temperature from 19.5 to 15.5 K. The data in both phases were also used to calculate the Poisson ratio, bulk and shear moduli, the distribution of the acoustic velocities in high-symmetry planes, and the Debye temperature. Raman spectra of the fundamental modes ν_1 and ν_3 were recorded and their shifts and full widths at half height were determined as a function of temperature through the phase transition. [S0163-1829(98)05429-0]

I. INTRODUCTION

The discovery of helium by Janssen and Lockyer in 1868 and argon by Rayleigh and Ramsay[1] ultimately created a new field of interest in physics—rare-gas solids (RGS). These solids have been and still are the subject of a wide range of experiments, for the molecular-dynamic simulations and for testing the predictions of lattice-dynamics theories. In many respects the inert gases form the simplest crystals known. These crystals are composed of atoms with completely filled electron shells and have spherically symmetric distributions of electronic charge. They all have a face-centered-cubic (fcc) structure with the exception of He^3 and He^4 (which also have fcc structure at higher pressures.[2]) These solids also were the first materials that were subject to methodical study by Brillouin spectroscopy.[3–6]

The considerable progress that has been made in understanding the properties of the RGS has provided impetus for theoretical and experimental research on more complex systems such as molecular crystals. The molecular crystals are much more complicated systems than the RGS. Among them, methane is archetypal because, with increasingly complicated crystal structure and intermolecular forces, it still remains a relatively simple compound. Just like the RGS, methane forms a cubic fcc lattice with van der Waals interaction between molecules, it has closed electron shells, and is almost spherically symmetric. Crystalline methane is of particular interest because it belongs to a class of materials where the constituent molecules are orientationally disordered (OD) over a wide temperature range.

The properties of methane are also of interest for a number of other reasons. It is the major constituent (up to 97%) of natural gas found on earth.[7] It also is a significant hydrocarbon constituent of several planetary bodies in the solar system. Condensed CH_4 (possibly crystalline) has been identified on Pluto[8] and Neptune's moon Triton.[9] Condensed CH_4 is expected to exist on Uranus[10] and Neptune.[11]

Knowledge of the elastic properties is clearly of interest in the latter context. Such information can also provide a key to understanding the microscopic properties of the orientational disorder, and the rotation-translation (RT) coupling mechanism.[12] RT coupling is the interaction between the center-of-mass displacements and large-amplitude orientational motion that may occur in molecular crystals, or crystals with molecular ions, and may cause a change in the state of orientational (dis)order. Such effects are of particular interest with respect to phase transitions.

Methane and its deuterated species have been under investigation in spectroscopic,[13–27] ultrasonic,[28] calorimetric,[29] neutron scattering,[30–34] and x-ray[35–42] experiments. Also, there was a series of theoretical papers on methane[43–54] and molecular-dynamics simulations.[55] The experiments yielded important information about the phase transition and attempts were made to describe both phases of methane at low temperature. But there were insufficient data on the elastic properties of methane and its deuterated compounds due to the difficulties in growing optically accessible single crystals of these compounds and maintaining them in an unstrained state in both phases. To date only a few experiments on the elastic properties of methane have been published.[20,27,33] Some values of elastic constants obtained by different techniques for CH_4 and CD_4 are given in Table I. It can be seen that much more work has been done on heavy methane although there are likewise no consistent data for CD_4 over a wide temperature range.

In contrast to the rare-gas solids, for which good agreement between experimental and calculated values of elastic constants has been shown,[3,4,6,56–64] there are difficulties in dealing with molecular solids such as methane. For example, for krypton and argon, whose physical characteristics are close to methane, elastic constants have been determined and the phonon-dispersion curves along high-symmetry directions have been measured[59,64] in good agreement with theoretical calculations. In Table II ratios of sound velocities in high-symmetry directions and anisotropy factor A of the rare-gas solids[65] are compared with those for OD crystals of molecular solids. It can be seen that all the ratios V_l/V_t are the same to within a few percent with the exception of V_l/V_t in

TABLE I. Comparison of experimental and theoretical values of elastic constants (kbar) of CH_4 and CD_4. The temperatures T are in Kelvins, and the elastic constants are in units of kbar unless otherwise noted.

CH_4	T	C_{11}	C_{12}	C_{44}	Ref.
Brillouin spectra	90.4	19.57 ± 0.30	14.46 ± 0.20	9.20 ± 0.15	20
Molecular dynamics	91.0	16.40 ± 1.00	13.60 ± 1.00	6.00 ± 0.30	55
Brillouin spectra[a]	300	10–25	8–23	4–7	27
CD_4					
Brillouin spectra	89.2	20.04 ± 0.30	15.00 ± 0.24	9.15 ± 0.15	20
Neutron scatt.	32.5	30.80 ± 2.00	21.40 ± 2.40	15.8 ± 0.60	33
Born–von Karman	32.5	34.10	26.8	14.20	33
Lennard-Jones	34.5	30.70	16.40	18.6	30
Neutron scatt.	34.5	32.80 ± 1.6	23.90 ± 1.6	14.9 ± 1.0	30

[a]The values of elastic constants are in GPa. Pressure was varied from 1 to 5 GPa.

the $\langle 110\rangle$ direction for OD crystals where V_l/V_t is higher by $\sim 25\%$ in CH_4, CD_4, CBr_4, and enormously high in CCl_4, which is a fascinating substance with respect to RT by itself. This anomaly is due to a low value of V_t in the $\langle 110\rangle$ direction and sometimes is called ''transverse mode softening.'' A similar comment applies to the anisotropy factor which is $\sim 30\%$ larger in OD crystals than in RGS. This is a direct consequence of RT coupling.

Most recently, a theoretical approach to RT coupling was undertaken by Lynden-Bell and Michel.[66] They have shown that RT coupling is caused by the changes in orientational potential felt by a molecule when it or nearby molecules or atoms move. The amount of this change depends on the actual strength and form of the intermolecular potential. They also showed that RT coupling in orientationally disordered crystals can influence phase transitions, affect the value of elastic constants, and change the appearance of phonon spectra.

Unlike its fully deuterated species, which exists in three different solid phases under its own vapor pressure, normal methane CH_4 exists only in phase I (space group $Fm3m$)[31,67] which extends from the melting point of 90.67 K to $T_c=20.5$ K, and in phase II (space group $Fm3c$)[31,67] at temperatures below T_c. Phase I is fcc with four molecules per unit cell. In this phase all molecules are free to rotate and there is no orientational order. Phase II is also fcc but the transition to this phase involves the ordering of six out of eight molecules.[31,67] The objective of the present work was to obtain consistent values of elastic constants over a wide range of the temperature and including phase II. Phase III exists only at higher pressures and it was not investigated in the present experiment.

TABLE II. Ratios of sound velocities in high-symmetry directions and anisotropy factor of the rare-gas solids compared with those for orientationally disordered crystals.

Crystal	T(K)	$\langle 100\rangle$ V_l/V_t	$\langle 111\rangle$ V_l/V_t	$\langle 110\rangle$ V_l/V_{t1}	$\langle 110\rangle$ V_l/V_{t2}	A	Ref.
Ar	80.0	1.46	2.27	1.66	2.75	2.73	4
Ne	24.0	1.40	2.20	1.61	2.66	2.74	5
Kr	115.6	1.45	2.26	1.66	2.73	2.70	6
Xe	160.0	1.44	2.24	1.65	2.71	2.74	3
CCl_4-(Ia)	244.1	1.79	3.07	2.01	4.70	3.48	80
CBr_4-I	333.0	1.62	2.65	1.83	3.54	3.73	81
CH_4-I	90.4	1.46	2.44	1.69	3.20	3.60	20
CD_4-I	89.2	1.48	2.47	1.71	3.25	3.63	20

II. EXPERIMENTAL TECHNIQUE

A. Raman technique

There is an abundance of Raman data for liquid[16,13] and polycrystalline[19,21] methane at different pressures and temperatures, but there is relatively little Raman data pertaining to phase transitions and RT coupling in single crystals. The present experiment was consequently designed to conduct the Raman spectroscopy experiment simultaneously with the Brillouin investigations. Raman measurements were made using a cooled RCA C31034 photomultiplier tube and a Spex model 1401 double-grating spectrometer, which was modified for computer control and data acquisition.

A schematic optical diagram for the Raman experiment is shown in Fig. 1. The optical axis of the spectrometer was perpendicular to the y axis of the laboratory reference frame which was defined by a He-Ne laser beam. The incident (vertical) beam of the argon laser defined the laboratory z axis. The scattered light was collected horizontally through a polarizer P by a collecting lens, L_1. Then, the light was focused by the lens L_2 on to a polarization scrambler S, in order to compensate for the different polarization sensitivities of the spectrometer. The frequency calibrations were done with a hollow-cathode thorium/neon discharge tube.

B. Brillouin technique

The Brillouin technique used for determining the elastic constants is very well known and documented.[68–70,65] It is based on the inelastic scattering of the incident light on the thermal acoustic waves propagating in the scattering media. The scattered light is Doppler shifted and the shift is described by the Brillouin equation:

$$\Omega = \pm 2n\frac{V}{\lambda}\sin\left(\frac{\theta}{2}\right), \tag{1}$$

where Ω is a frequency shift, n is the refractive index of the crystal, θ is the scattering angle and λ and V are the wave-

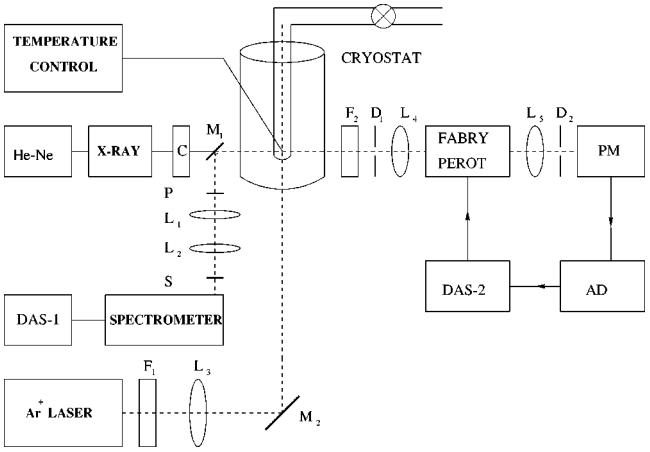

FIG. 1. Experimental setup: F_1 is a narrow band pass filter, L_3 is a focusing lens, He-Ne is the alignment laser, M_2 is a mirror, C is the x-ray collimator, Ar^+ is the argon laser. (a) Raman part: $L_{1,2}$ are lenses, DAS-1 is the data acquisition system, P is the polarizer, S is the scrambler. (b) Brillouin part: PM is the photomultiplier tube, AD is the amplifier discriminator, F_2 is a narrow band pass filter, $L_{4,5}$ are lenses, $D_{1,2}$ are pinholes, DAS-2 is the data acquisition system.

length of the incident light and sound velocity, respectively. The relation between the frequency shifts and elastic constants is given by a secular equation, known as a Christoffel determinant:

$$|C_{ijkl}n_j n_l - \rho V^2 \delta_{ik}| = 0. \tag{2}$$

This is a cubic equation for ρV^2, where ρ is the density. Three roots of this equation correspond to the three polarization vectors of the acoustic modes which, for the high-symmetry directions $\langle 100 \rangle$, $\langle 110 \rangle$, and $\langle 111 \rangle$, correspond to one longitudinal (the one with the highest velocity) and two transverse modes. In other directions the modes can be described by their predominant polarization as ''quasilongitudinal'' or ''quasitransverse.'' These roots are functions of the elastic constants and the direction cosines of the crystal. The direction cosines are related to the laboratory frame via the Euler angles θ, ϕ, and χ, which can be determined by x-ray diffraction techniques. Once the orientation of the crystal is known, a nonlinear least-squares fitting routine can be applied to the combined equations (1) and (2) to determine the elastic constants. The procedure starts with an initial guess for the elastic constants. The values of elastic constants are put into the Cristoffel determinant and then determinant is solved, yielding the values for ρV^2. The values for V are used to calculate the frequency shifts using the Brillouin equation and the calculated frequencies are compared with the measured ones. A least-squares fitting routine is then applied to minimize the difference between the calculated and measured frequency shifts. The quantity χ^2 which is minimized by the parameter searches through the elastic-constant space is determined by

$$\chi^2 = \sum_{i=1}^{N} \left(\frac{\nu_i^{\text{calc}} - \nu_i^{\text{obs}}}{\sigma_i} \right)^2, \tag{3}$$

where N is the total number of the measurements at a given temperature and σ is the experimental uncertainty.

A schematic optical diagram for the Brillouin experiment is shown in Fig. 1. A (20 mW, 514.5 nm) laser beam from a Spectra Physics Series 2000 single-mode argon laser was incident vertically along the axis of the cell. The scattered light of interest was collected horizontally through a narrow band pass filter, F_2, by a collecting lens, L_4. The collimated beam was then incident on a piezoelectrically scanned, triple-pass Fabry-Perot interferometer (FP) with a finesse and spectral free range of 50 and 18.20 GHz, respectively. The light from the Fabry-Perot was focused by lens L_5 through a pinhole D_2 on to the cathode of an ITT FW 130 photomultiplier tube (PM) operating in photon counting mode. The signal from the photomultiplier was passed to a computer-controlled data acquisition system (DAS-2) through an amplifier discriminator, AD. The DAS-2 stored the spectrum in a 1280 multichannel memory, displayed the spectrum on the screen, and performed all functions required to control the scanning of the interferometer. The optic axis of the spectrometer and the y axis of the laboratory reference frame were coincident and were both defined by a He-Ne laser beam. The incident (vertical) beam of the argon laser defined the laboratory z axis. The axis of the x-ray machine was aligned with the optic axis to ensure that the radiation passed through the region of the crystal at the focus of lens L_4.

C. Sample preparation

The CH_4 gas used in the experiment was of research-grade quality (Matheson, minimum purity 99.99%). The tubular quartz cell containing the gas was mounted in a liquid-helium cryostat and was rotatable about the vertical axis. The cell was filled to a pressure of approximately 350 Torr and then the gas was liquefied and cooled to $\sim$91 K. Large ($\sim$50 mm^3) single crystals of CH_4 were then grown from the liquid.

During the first stage of this process crystals were generally grown by lowering the temperature of the cell very slowly (0.005–0.1 K per hour) in the presence of a temperature gradient ($\sim$1 K/cm) between the top and the bottom of the cell until a small seed was formed on the bottom. This procedure usually took around 10–12 h. X-ray Lauë diffraction photographs were then taken to ensure that the crystal seed was single and of good quality. These photographs were also used to determine the orientation of the crystal.

Next the crystal was prepared for cooling to the desired temperature. Cooling a van der Waals solid is very difficult because the combination of a high coefficient of thermal expansion and strong adhesion to the cell wall usually results in fracturing of the crystal after even a modest drop in temperature. This problem was circumvented in the experiment by employing an electrically conducting and optically transparent film deposited on the exterior walls of the cell. By applying a voltage across this film (from top to bottom), and simultaneously removing methane vapor from the cell by pumping, it was possible to separate the crystal from the cell walls. This required a delicate balance between the rate of pumping, raising the film voltage and lowering the temperature. When successful, the result was a crystal standing freely on the bottom (window) of the cell. Subsequently the temperature of the cell could sometimes be lowered automatically by as much as 10 K per hour to any desired value

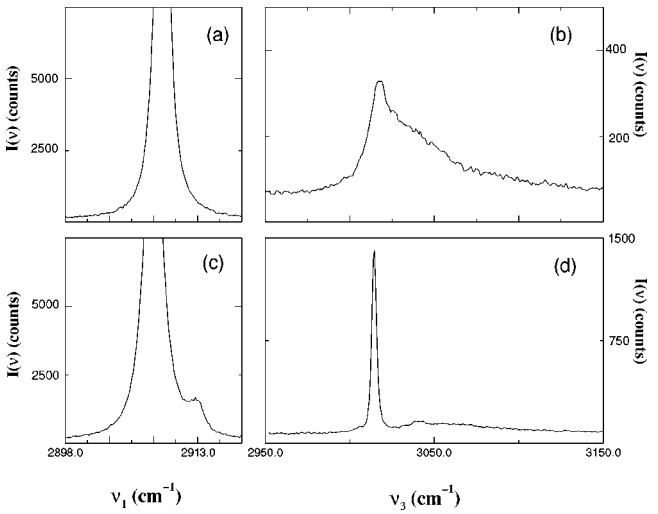

FIG. 2. Typical Raman spectra of ν_1 and ν_3 of CH_4. (a) and (c) show the ν_1 spectrum in phases I and II, respectively, and (b) and (d) are corresponding spectra for ν_3. ν_3 was recorded with the polarizer axis perpendicular to the polarization vector of the incident laser beam.

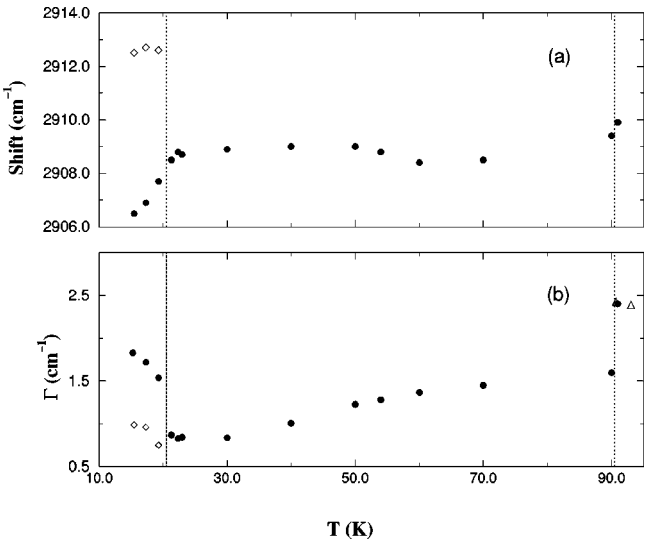

FIG. 3. The shift (a) and full width at half height (b) of ν_1 as a function of temperature. ($\diamond$) indicates the second peak which appeared after the phase transition. ($\triangle$) indicates values from Ref. 73. The errors in measurements of shift are comparable to the symbol size. The errors in measurements of FWHM are estimated to be $\sim$2%. The dashed lines are positioned at the phase transition temperature of 20.5 K and at the liquid-solid phase boundary at 90.67 K.

without significant deterioration in crystal quality. Usually, however, there was some deterioration in crystal quality. At the lower temperature it is desirable to regrow the crystal against the walls but satisfactory results are extremely difficult to achieve.

III. RESULTS

A. Raman scattering

It is well known that a methane-like five-atomic tetrahedral molecule has four fundamental vibrational modes:[71] a totally symmetric $\nu_1(A_1)$, a doubly degenerate $\nu_2(E)$, and two triply degenerate $\nu_3(F_2)$ and $\nu_4(F_2)$. ν_4 also is infrared active but was not observed in this experiment. Attempts to detect the (external) lattice modes in phase II were unsuccessful. Only the ν_1 and ν_3 features were consistently observed over the investigated temperature range, and some representative spectra for both phases are shown in Fig. 2. It can be seen that the phase transition is readily detected via the splitting of the ν_1 feature and the more dramatic narrowing of ν_3. Corresponding spectra were recorded for different crystal orientations but there were no detectable differences.

The full width at half maximum (FWHM) of ν_1 was determined by employing a deconvolution process to correct for the finite spectrometer resolution. In this process the observed profiles for both the Raman line and the laser (instrumental) line were first fitted with Lorentzian functions. In both cases the quality of the fits was excellent and the primary effect was one of smoothing. The Fourier (cosine) coefficients were then determined for each fitted function and deconvolution was achieved by simply dividing the corresponding coefficients. The corrected spectrum was then obtained as the inverse Fourier transform.[72] The resulting profiles were then fitted to a Lorentzian line shape and the position of the peak and its FWHM were deduced. The results for the ν_1 line are shown in Fig. 3. The points for liquid CH_4 from Ref. 73 were measured using Fabry-Perot interferometry and are consistent with the present measurements. The Raman shift values (Fig. 3) are consistently higher by $\sim$3 cm^{-1} than those of Ref. 15. There is little change in the shift throughout the temperature range of phase I, but there is a distinct downshifting effect on entering phase II. The most interesting effect is the widening of the main peak of ν_1 when the crystal goes through the phase transition. The width of the peak changes from 1.6 to 0.87 cm^{-1} through the temperature range of phase I. On passing through the phase transition at 20.5 K it jumps to 1.57 cm^{-1} and continues to rise as the temperature is further reduced. Assuming, as suggested elsewhere (Ref. 74), that the principal broadening mechanism in phase I is fast-modulation dephasing, it is likely that the increased width in phase II is due to an inhomogeneous broadening contribution arising from the $(Fm3c)$ ordering.

In order to calculate the linewidth of ν_3 it is necessary to eliminate the line $2\nu_2$. Because ν_3 is completely depolarized and $2\nu_2$ is completely polarized this can be achieved by employing a polarizer (see Fig. 2). The width of the ν_3 feature averages about 70 cm^{-1} in phase I, and instrumental linewidth contributions were not significant in this case. The changes in ν_3 are the most obvious ones observed in this experiment (Fig. 4). The Raman shift changes from 3026 cm^{-1} at 90 to 3016.9 cm^{-1} at 20.5 K and then it downshifts to 3014.5 cm^{-1} in phase II. The ν_3 linewidth changes by a factor of 3 from 90 to 20.5 K and when the crystal goes through the phase transition it suddenly decreases from 34 to 4.6 cm^{-1}. This latter effect was a sensitive test of whether the phase transition had actually occurred. In some cases a distinct ''overcooling'' effect was observed when the temperature was well below the normal phase-transition temperature but the linewidth and height of ν_3 clearly indicated that the phase transition had not occurred. A light tapping on the cryostat would then initiate the phase transition which

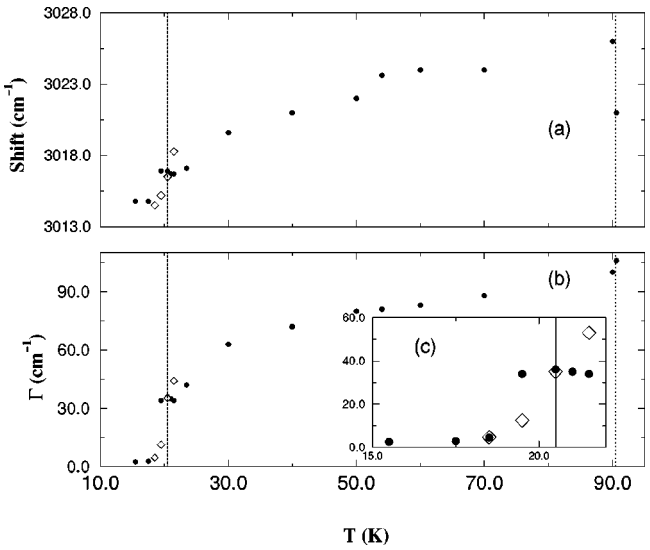

FIG. 4. The shift (a) and full width at half height (b) of ν_3 as a function of temperature. The (●) symbols are for decreasing and the (◇) symbols for increasing temperatures, respectively. The inset (c) shows a magnified view of FWHM around the phase-transition temperature. The errors in measurements of shift are comparable to the symbol size. The errors in measurements of FWHM are estimated to be ~2%. The dashed lines are positioned as in Fig. 3.

would be complete within a few minutes. An attempt was made to observe the associated hysteresis effect in the behavior of a linewidth corresponding to that demonstrated in the enthalpy measurements of Ref. 29. The single point at 18.5 K in Fig. 4(c) suggests the existence of such an effect but more precise measurements of the sample temperature are needed in order to confirm it.

B. Brillouin scattering

In phase I more than 15 independent crystals were studied, but only three were successfully cooled below the phase-transition temperature. Because of the development of internal defects, the quality of spectra tended to deteriorate with decreasing temperature and some orientations produced better spectra than others. As a general rule spectra were measured in 5° or 10° intervals through 70° in the angle ϕ.

Both the density and refractive index of a crystal are needed for calculating the elastic constants from the Brillouin frequency shifts. The refractive index of solid methane at the triple point is known[20] and equal to 1.323. The density is also known for the 90–10 K temperature range.[39] The Lorentz-Lorenz relation was consequently used to calculate refractive indices over the wide temperature range required. The resulting values of the elastic constants for both phases of solid methane are listed in Table III and plotted (solid circles) versus temperature close to the phase-transition point in Fig. 5. This figure also includes least-squares linear fits to the plotted values for each elastic constant. It is interesting to note that C_{44} and C_{11} have steeper slopes than C_{12}. Consequently, C_{44} becomes comparable with C_{12} at the temperatures close to the phase transition and in phase II. In phase II the slopes and values of C_{12} and C_{44} are almost equal, although no firm conclusions can be made owing to the small number of experimental points. The dependences of the elastic constants on temperature, as determined by the linear fits in phase I are

TABLE III. Elastic constants of CH_4 in phase I and II in kbars. Temperatures are accurate to within ±0.2 K.

T(K)	C_{11}	C_{12}	C_{44}
		Phase I	
90.0	19.6±0.2	14.8±0.1	9.2±0.1
70.0	23.8±0.3	16.9±0.3	11.5±0.2
60.0	25.4±0.2	17.7±0.2	12.6±0.2
54.0	26.7±0.2	18.2±0.2	13.3±0.1
50.0	27.2±0.2	18.3±0.2	13.9±0.1
48.1	26.7±0.2	18.3±0.2	14.1±0.1
38.0	28.9±0.3	19.4±0.2	15.6±0.2
30.0	29.7±0.3	18.8±0.2	15.8±0.2
26.1	29.5±0.3	19.4±0.2	16.9±0.2
25.0	30.2±0.3	19.4±0.2	16.7±0.2
24.8	30.1±0.3	19.3±0.2	18.2±0.2
23.0	30.0±0.3	19.2±0.2	16.5±0.3
22.3	31.1±0.3	19.0±0.2	18.1±0.2
21.3	30.4±0.3	19.5±0.3	18.6±0.2
20.5	31.4±0.3	19.8±0.2	18.8±0.2
		Phase II	
19.3	30.9±0.3	18.1±0.2	19.3±0.3
17.3	33.9±0.3	19.0±0.3	18.7±0.3
15.5	34.0±0.3	19.3±0.2	19.4±0.2

$$C_{11}(T) = -0.149T + 34.02, \tag{4}$$

$$C_{12}(T) = -0.059T + 20.93, \tag{5}$$

$$C_{44}(T) = -0.128T + 20.41. \tag{6}$$

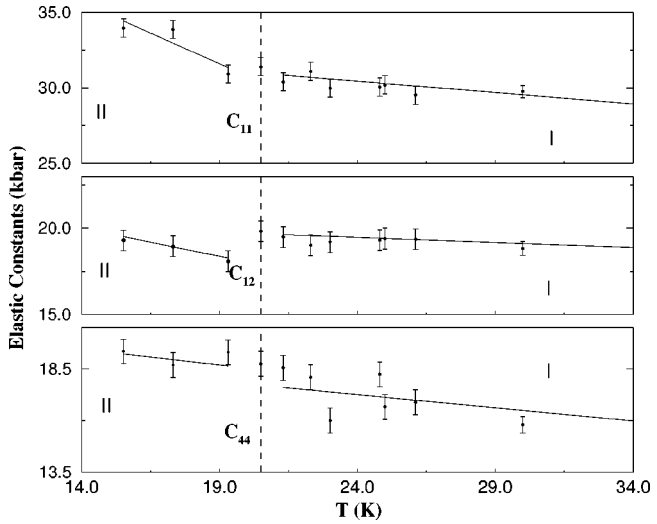

FIG. 5. Elastic constants of CH_4 as a function of temperature. The error bars shown represent the standard deviation in the best fit parameters and uncertainties in the frequency shift and crystal orientation. The dashed line is positioned at the phase-transition temperature of 20.5 K. The solid lines in the phase II are drawn only as guides to the eye.

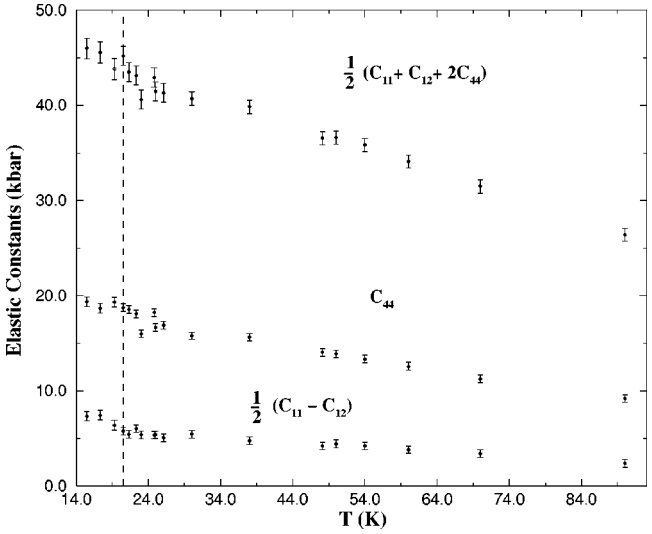

FIG. 6. Elastic constants of CH_4 as a function of temperature. The combinations correspond to the longitudinal and two transverse waves in the $\langle 110 \rangle$ direction. The error bars shown are from the errors in elastic constants as in Fig. 5. The dashed line is positioned as in Fig. 5.

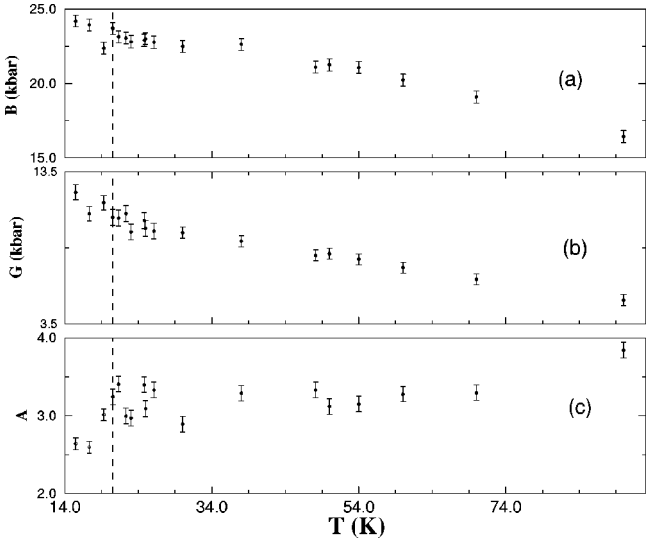

FIG. 7. Elastic moduli and anisotropy factor of CH_4 as a function of temperature. (a) Bulk modulus. (b) Shear modulus. (c) Anisotropy factor. The error bars shown are from the errors in elastic constants as in Fig. 5. The dashed line is positioned as in Fig. 5.

There are no significant changes in the elastic constants when the crystal goes through the phase transition but temperature dependences are noticeably different for C_{11} and C_{12}.

The combinations of elastic constants corresponding to the $\langle 110 \rangle$ direction are shown in Fig. 6. The $\frac{1}{2}(C_{11}-C_{12})$ and C_{44} plots correspond to two shear moduli in the cubic structure.

With elastic constants known, the bulk modulus was calculated as

$$B=\frac{1}{3}(C_{11}+2C_{12}). \tag{7}$$

The aggregate shear modulus $(G)$was obtained from the Voight-Reuss-Hill averaging method.[75] These parameters are shown in Figs. 7(a) and 7(b). The bulk modulus increases by a factor 1.5 and the shear modulus increases by a factor of 2 with decreasing temperature over the investigated range. There are no noticeable changes in the values of elastic moduli such as B, $(C_{11}-C_{12})/2$ and C_{44} when passing through the phase transition. The phase transition was confirmed by the observation of changes in the ν_1 and ν_3 modes of the vibrational Raman spectra.

Lynden-Bell and Michel[66] have showed that softening of the elastic constants can occur via rotation-translation coupling at the Γ point ($\vec{\mathbf{k}}=0$) as a result of coupling to the $L=4$ rotator function. They anticipated that the effect would be comparatively small due to the high value of L involved and that it should not be affected by the phase transition. This is indeed what is observed in the present experiment: all three elastic constants show small increases with decreasing temperature, and there is no significant effect at the phase transition.

The most notable changes are associated with the anisotropy factor A,

$$A=\frac{2C_{44}}{C_{11}-C_{12}}, \tag{8}$$

and the quantity $\delta=(C_{12}-C_{44})/C_{12}$. The latter is a measure of the extent to which the Cauchy relation,[54] $C_{44}=C_{12}$, is violated and, in turn, indicates the level of importance of noncentral forces between molecules. Both quantities are plotted as a function of temperature in Figs. 7(c) and 8(a). As the temperature is decreased, A decreases from 4 to ~ 2.5, and δ decreases from ~ 0.4 to ± 0.05. The A value compares very closely with the RGS at temperatures below the phase transition and, when taken in conjunction with $\delta \sim 0$, suggests that the lattice dynamics can be described quite well by nearest-neighbor central forces.

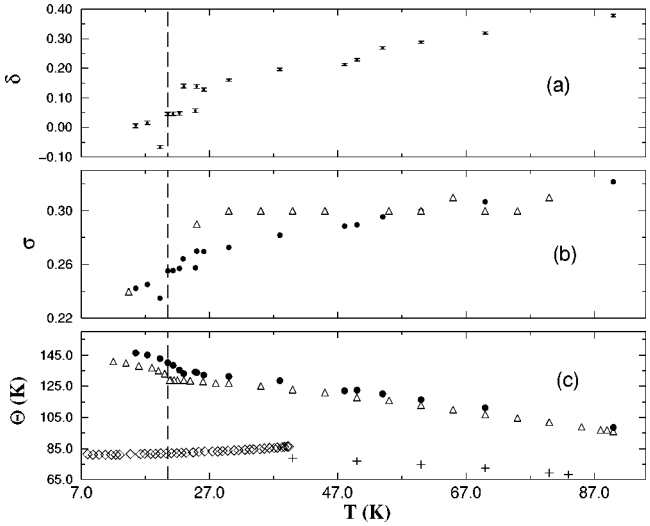

FIG. 8. (a) $\delta=(C_{12}-C_{44})/C_{12}$ as a function of temperature. (b) Poisson ratio σ. The $(\triangle)$ are from Ref. 76. (c) Debye temperature of solid CH_4 $(\bullet)$. Compared with results $(\triangle)$ from Ref. 39 and $(\diamond)$ Debye temperature of solid argon from Ref. 78 and $(+)$ Ref. 79. The dashed line is positioned as in Fig. 5.

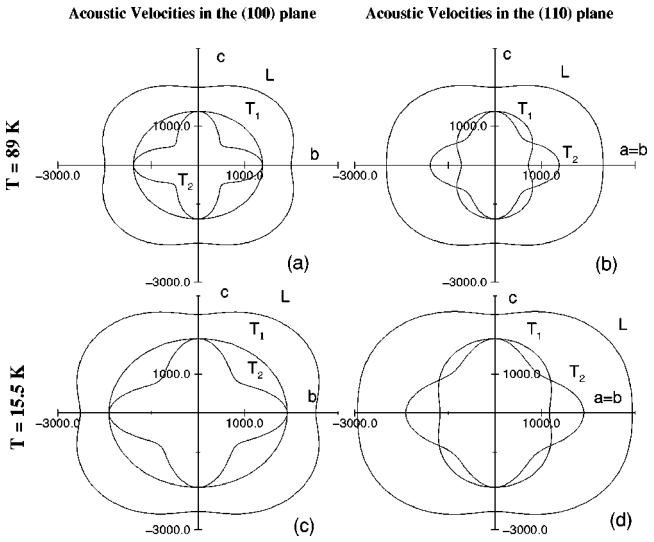

FIG. 9. Acoustic velocities (in ms^{-1}) in high-symmetry planes. (a) and (b) are at 89 K (phase I). (c) and (d) are at 15.5 K (phase II). (a) and (c) are in the (100) plane, (b) and (d) are in the (110) plane.

Having determined the complete set of elastic constants, the acoustic velocity can be calculated for any propagation direction. As an example the acoustic velocities for all directions in the (100) and (110) planes in both phases are shown in Fig. 9. Although C_{44} and C_{12} converge to the same value in phase II, there is no correspondingly significant effect in the angular dependence of the velocity. There is, however, a detectable tendency towards higher isotropy in phase II.

The Poisson ratio was calculated using the expression

$$\sigma = \frac{(V_l^2 - 2V_t^2)}{2(V_l^2 - V_t^2)}, \tag{9}$$

where V_l and V_t are the values averaged over the reciprocal velocity surfaces. The temperature dependence of the Poisson ratio is shown in Fig. 8(b) and compared with that from Ref. 76.

The Debye temperature was determined via the expression[77]

$$\theta_D = \left(\frac{6\pi^2 N}{V}\right)^{1/3} \frac{\hbar V_{\mathrm{av}}}{k_B}, \tag{10}$$

where $\hbar$ is Planck's constant, k_B is Boltzmann's constant, N is the Avogadro number, and V is the molar volume. In the above expression the mean velocity V_{av} was computed at each temperature by averaging over the three reciprocal velocity surfaces:

$$\frac{3}{V_{\mathrm{av}}^3} = \int \left[\frac{1}{V_l^3} + \frac{1}{V_{t1}^3} + \frac{1}{V_{t2}^3}\right] d\omega, \tag{11}$$

where ω is an element of solid angle. The resulting values of the Debye temperature are plotted versus temperature in Fig. 8(c), Also shown are the Debye temperatures obtained on the basis of x-ray measurements from Ref. 39. It can be seen [Fig. 8(c)] that the values of Debye temperature obtained in our experiment are consistently higher than in Ref. 39 but the dependence on temperature is essentially the same. Also, the Debye temperature of solid argon measured by calorimetric methods from Refs. 78 and 79 is shown for comparison.

IV. CONCLUSIONS

In this paper, a comprehensive study of solid methane was carried out using optical spectroscopic techniques at low temperatures. A technique for growing and cooling single crystals was developed and applied to the two phases of methane. The elastic properties were determined by the means of Brillouin spectroscopy. The wave numbers of internal modes and their linewidths were measured by the Raman scattering which clearly signaled the occurrence of the phase transition at 20.5 K. Such characteristics as the anisotropy factor and violation of the Cauchy relation in phase II were found to show some similarities between CH_4-II and rare-gas solids. The analysis of the behavior of Raman lines is consistent with partial quenching of rotational motion in phase II. The work is being extended to a study of solid heavy methane (CD_4) particularly in phase III.

ACKNOWLEDGMENTS

We would like to thank Dr. J. Zuk for his comments on the manuscript. The work was supported by a grant from the National Sciences and Engineering Research Council of Canada.

[1] Lord Rayleigh and W. Ramsay, Proc. R. Soc. London **57**, 265 (1895).
[2] D. Young, *Phase Diagrams of the Elements* (University of California Press, Berkeley, 1991).
[3] W. Gornall and B. Stoicheff, Phys. Rev. B **4**, 4518 (1971).
[4] S. Gewurtz and B. P. Stoicheff, Phys. Rev. B **10**, 3487 (1974).
[5] R. McLaren, H. Kiefte, D. Landheer, and B. Stoicheff, Phys. Rev. B **11**, 1705 (1975).
[6] D. Landheer *et al.*, Phys. Rev. B **13**, 888 (1976).
[7] R. Morrison and R. Boyd, *Organic Chemistry* (Allyn and Bacon, Boston, 1964).
[8] M. Buie *et al.*, Bull. Am. Astron. Soc. **21**, 985 (1989).
[9] D. Cruikshank *et al.*, Icarus **74**, 413 (1988).
[10] G. Lindal *et al.*, J. Geophys. Res. **92**, 14 987 (1987).
[11] B. Smith *et al.*, Science **246**, 1422 (1989).
[12] K. H. Michel and J. Naudts, J. Chem. Phys. **67**, 547 (1977); **68**, 216 (1978).
[13] M. F. Crawford, H. L. Welsh, and J. H. Harrold, Can. J. Phys. **30**, 81 (1952).
[14] A. Cabana, G. Savitsky, and D. Hornig, J. Chem. Phys. **39**, 2942 (1963).
[15] A. Anderson and R. Savoie, J. Chem. Phys. **43**, 3468 (1965).
[16] A. J. Rest, R. Warren, and S. C. Murray, Spectrochim. Acta **52**, 1455 (1966).
[17] A. Cabana and N. Thé, Can. J. Phys. **55**, 3862 (1977).
[18] D. Fabre, M. M. Thiery, H. Vu, and K. Kobashi, J. Chem. Phys. **71**, 3081 (1979).
[19] F. D. Medina J. Chem. Phys. **73**, 77 (1980).

[20] S. C. Rand and B. P. Stoicheff, Can. J. Phys. **60**, 287 (1982).
[21] D. Fabre, M. M. Thiery, and K. Kobashi, J. Chem. Phys. **76**, 4817 (1982).
[22] M. M. Thiery, D. Fabre, and K. Kobashi, J. Chem. Phys. **83**, 6165 (1985).
[23] P. Hebert *et al.*, Phys. Rev. B **36**, 9196 (1987).
[24] P. Calvani, S. Cunsolo, S. Lupi, and A. Nucara, J. Chem. Phys. **96**, 7372 (1992).
[25] R. Bini, L. Ulivi, H. Jodl, and P. Salvi, J. Chem. Phys. **103**, 1353 (1995).
[26] Y. Wu, S. Sasaki, and H. Shimizu, J. Raman Spectrosc. **26**, 963 (1995).
[27] S. Sasaki, N. Nakashima, and H. Shimizu, Physica B **219&220**, 380 (1996).
[28] S. V. Marx and R. O. Simmon, J. Chem. Phys. **81**, 944 (1984).
[29] J. H. Colwell, E. K. Gill, and J. A. Morrison, J. Chem. Phys. **39**, 635 (1963).
[30] W. Press, B. Dorner, and H. H. Stiller, Solid State Commun. **9**, 1113 (1971).
[31] W. Press and A. Huller, in *Anharmonic Lattices, Structural Transitions and Melting*, edited by T. Rieste (Noordhoff, Noordhoff–Leiden, 1974), p. 185.
[32] W. Press and A. Kollmar, Solid State Commun. **17**, 405 (1975).
[33] W. G. Stirling, W. Press, and H. H. Stiller, J. Phys. C **10**, 3959 (1977).
[34] M. Prager *et al.*, J. Chem. Phys. **75**, 1442 (1981); **77**, 2577 (1982).
[35] D. Aadsen, Ph.D. thesis, University of Illinois at Urbana-Champaign, 1975.
[36] D. R. Baer, B. A. Fraass, D. H. Riehl, and R. O. Simmons, J. Chem. Phys. **68**, 1411 (1978).
[37] I. Krupskii, A. Prokhvatilov, and A. Isakina, Sov. J. Low Temp. Phys. **8**, 317 (1982).
[38] I. Krupskii, A. Prokhvatilov, and A. Isakina, Solid State Commun. **42**, 59 (1982).
[39] A. Prokhvatilov and A. Isakina, Sov. J. Low Temp. Phys. **9**, 213 (1983).
[40] A. Prokhvatilov and A. Isakina, Phys. Status Solidi A **78**, 147 (1983).
[41] A. Prokhvatilov and A. Isakina, Sov. J. Low Temp. Phys. **10**, 631 (1984).
[42] A. Prokhvatilov and A. Isakina, Sov. J. Low Temp. Phys. **10**, 91 (1984).
[43] H. M. James and T. A. Keenan, J. Chem. Phys. **31**, 12 (1959).
[44] T. Yamamoto, J. Chem. Phys. **48**, 3193 (1968).
[45] T. Yamamoto and Y. Kataoka, J. Chem. Phys. **48**, 3199 (1968).
[46] Y. Kataoka and T. Yamamoto, Prog. Theor. Phys. Suppl. Extra Number 436 (1968).
[47] H. Yasuda, T. Yamamoto, and Y. Kataoka, Prog. Theor. Phys. **41**, 859 (1969).
[48] K. Nishiyama, Y. Kataoka, and T. Yamamoto, Prog. Theor. Phys. **43**, 1121 (1970).
[49] Y. Kataoka, Prog. Theor. Phys. **43**, 1132 (1970).
[50] H. Yasuda, Prog. Theor. Phys. **45**, 1361 (1971).
[51] A. Huller, Phys. Rev. B **10**, 4403 (1974).
[52] K. Michel and D. Kroll, J. Chem. Phys. **64**, 1300 (1976).
[53] T. Yamamoto, Y. Kataoka, and K. Okada, J. Chem. Phys. **66**, 2701 (1977).
[54] S. Wonneberger and A. Huller, Z. Phys. B, **66**, 191 (1987).
[55] D. G. Bounds, M. L. Klein, and G. N. Patey, J. Chem. Phys. **72**, 5348 (1980).
[56] Y. Fujii *et al.*, J. Phys. Chem. Solids **36**, 145 (1975).
[57] R. Fisher and R. Watts, Mol. Phys. **23**, 1051 (1972).
[58] J. Skalyo and Y. Endoh, Phys. Rev. B **7**, 4670 (1973).
[59] J. A. Barker, M. L. Klein, and M. Bobetic, Phys. Rev. B **2**, 4176 (1970).
[60] A. Huller, Z. Phys. **245**, 324 (1971).
[61] H. Peter *et al.*, J. Phys. Chem. Solids **34**, 255 (1973).
[62] M. L. Klein and R. Murphy, Phys. Rev. B **6**, 2433 (1972).
[63] N. Lurie *et al.*, Phys. Rev. B **9**, 2661 (1974).
[64] J. Skalyo, Y. Endoh, and G. Shirane, Phys. Rev. B **9**, 1797 (1974).
[65] B. Stoicheff, in *Rare Gas Solids I and II*, edited by M. L. Klein and J. A. Venables (Academic, London, 1977), p. 979.
[66] R. M. Lynden-Bell and K. H. Michel, Rev. Mod. Phys. **66**, 721 (1994).
[67] W. Press, J. Chem. Phys. **56**, 2597 (1972).
[68] G. Benedek and K. Fritsch, Phys. Rev. **149**, 647 (1966).
[69] R. Vacher and L. Boyer, Phys. Rev. B **6**, 639 (1970).
[70] H. Kiefte and M. J. Clouter, J. Chem. Phys. **62**, 4780 (1975).
[71] G. Herzberg, *Molecular Spectra and Molecular Structure* (Van Nostrand, New York, 1960).
[72] E. Hecht, *Optics* (Adison-Wesley, Reading, 1979).
[73] M. J. Clouter, H. Kiefte, and C. G. Deacon, Phys. Rev. A **33**, 2749 (1986).
[74] M. J. Clouter, Annu. Rev. Phys. Chem. **39**, 69 (1988).
[75] Z. Hashin and S. Shtrikman, J. Mech. Phys. Solids **10**, 343 (1962).
[76] P. Bezuglyi, N. Burma, and R. Minyafaev, Sov. Phys. Solid State **8**, 596 (1966).
[77] N. Ashcroft and N. Mermin, *Solid State Physics* (Saunders College, Philadelphia, 1976).
[78] R. Beaumont, H. Chihara, and J. Morrison, Proc. Phys. Soc. London **78**, 1462 (1961).
[79] O. Rice, *Statistical Mechanics Thermodynamics and Kinetics* (W.H. Freeman and Company, San Francisco, 1967).
[80] J. Zuk, H. Kiefte, and M. Clouter, J. Chem. Phys. **92**, 917 (1990).
[81] J. Zuk, D. Brake, H. Kiefte, and M. Clouter, J. Chem. Phys. **91**, 5285 (1989).